

Interactive Uncertainty Allocation and Tradeoff for Early-stage Design of Complex Systems

Arturo Molina-Cristóbal¹, Xin Chen², Marin D. Guenov³, Atif Riaz² and Albert S.J. van Heerden²

*School of Aerospace, Transport, and Manufacturing
Cranfield University, Cranfield, Bedfordshire, MK43 0AL, United Kingdom*

A common probabilistic approach to perform uncertainty allocation is to assign acceptable variability in the sources of uncertainty, such that pre-specified probabilities of meeting performance constraints are satisfied. However, the computational cost of obtaining the associated tradeoffs increases significantly when more sources of uncertainty and more outputs are considered. Consequently, visualizing and exploring the decision (trade) space becomes increasingly difficult, which, in turn, makes the decision-making process cumbersome for practicing designers. To address this problem, proposed is a parameterization of the input probability distribution functions, to account for several statistical moments. This, combined with efficient uncertainty propagation and inverse computation techniques, results in a computational system that performs order(s) of magnitude faster than a state-of-the-art optimization technique. The approach is demonstrated by means of an illustrative example and a representative aircraft thermal system integration example.

¹ Lecturer, Centre for Aeronautics, Cranfield, MK43 0AL, United Kingdom.

² Research Fellow, Centre for Aeronautics, Cranfield, MK43 0AL, United Kingdom, AIAA Member.

³ Professor, Head of the Centre for Aeronautics, Cranfield, MK43 0AL, United Kingdom, AIAA Senior Member.

Citation: Arturo Molina-Cristóbal, Xin Chen, Marin D. Guenov, Atif Riaz and Albert S. J. van Heerden, "Interactive Uncertainty Allocation and Tradeoff for Early Stage Design of Complex Systems," AIAA Journal, (2019). Article in Advance Published Online: 27 Nov 2019. <https://doi.org/10.2514/1.J058442>

Nomenclature

\mathbf{h} = Computational workflow, or model

$\mathbf{Y} = (y_1, \dots, y_J) \in \mathbb{R}^J$ is the vector of random output variables, or outputs of interest.

$\mathbf{X} = (x_1, \dots, x_I) \in \mathbb{R}^I$ is the vector of random input variables.

$f_{x_i}(x_i, \mathbf{d}_{x_i, p_i})$ is the probability density function (PDF) of the i^{th} input random variable.

\mathcal{A} is the design space domain.

$\mathbf{d}_{x_i, p_i} = (d_{x_i, 1}, \dots, d_{x_i, p_i}) \in \mathbb{R}^{p_i}$ is the vector of shape parameters that describe the shape of the input PDF, $f_{x_i}(x_i, \mathbf{d}_{x_i, p_i})$.

$\mathbf{d}_{y_j, p_j} = (d_{y_j, 1}, \dots, d_{y_j, p_j}) \in \mathbb{R}^{p_j}$ is the vector of parameters that describes the variability of the j^{th} output of interest

g_j = Constraint function of j^{th} output of interest

P_{g_j} = Pre-defined probabilities of satisfying j^{th} constraint

μ_x = Mean, first statistical moment

σ_x = Standard deviation, second statistical moment

γ_x = Skewness, third statistical moment

Γ_x = Kurtosis, fourth statistical moment

V_{cruise} = Cruise velocity

L/D = Lift-to-drag ratio

W_{empty} = Empty weight

W_p = Payload weight

W_f = Fuel weight

sfc = Specific fuel consumption

$Temp_{total}$ = Total mean temperature, over all equipment surfaces

$Temp_{PC}$ = Maximum surface temperature of the power center

$Temp_{BAT}$ = Maximum surface temperature of the battery

\dot{m}_{PC} = Air mass flow extracted from power center

$Temp_{Fus}$ = Fuselage reference temperature

$Temp_{NLG}$ = Nose landing gear (NLG) reference temperature

HTC = Factor of fuselage, NLG, cargo wall, floor heat transfer coefficient

$Heat_{diss}$ = Avionics equipment heat dissipation

1 INTRODUCTION

In order to make well-informed decisions early in the design stage, it is desirable to not only assess the impact of uncertainty due to a lack of knowledge, but also to reduce it [1],[2]. One approach is to quantify and assign acceptable variability in the sources of uncertainty. In this paper, this approach is referred to as ‘uncertainty allocation’. Allocating uncertainty is necessary to allow systems architects or designers to avoid situations where unknown variations in parameters or behaviors could lead to undesirable deviations in performance [2]. Uncertainty allocation is also useful for identifying different potential means of ensuring a desired probability of constraint satisfaction, or for assigning an appropriate tolerance limit for low-level geometrical characteristics. Our research, as part of recent and current industry led projects, including Thermal Overall Integrated Conception of Aircraft (TOICA) [3],[4] and Advanced Product Concept Analysis Environment (APROCON) [5], indicates that uncertainty allocation is indeed considered as part of the decision-making process. However, it is based predominantly on experience and, as a result, the decision-maker may not be aware of the full set of options available for tradeoff.

Current Uncertainty Quantification and Management (UQ&M) practices, such as robust design, optimization, and reliability analysis, involve minimizing or maximizing the outputs of interest (e.g., system performance), by systematically searching for design solutions that are robust against aleatory uncertainty and some classes of epistemic uncertainty (e.g., model uncertainty [6],[7]). While these approaches are effective in finding robust solutions, they are not suited to address the uncertainty allocation problem. Chen et al. [8] reported that inverse uncertainty propagation methods can be used as an enabler to solve the uncertainty allocation problem. Although several methods have been developed for inverse uncertainty propagation (e.g., the Gaussian process [9], Karhunen–Loève Expansion [10],[11], Polynomial Chaos [12], and maximum likelihood [13]) these may lead to relatively high computational cost.

The ‘inverse uncertainty propagation’ method introduced by Chen et al. [8] demonstrated that a reduction in variability can be achieved by reversing (swapping) the standard deviation of an input variable with one of the standard deviations of the original output variables. It cannot, however, deal with many-to-many reversals (i.e. multiple outputs with multiple inputs). Another limitation of this method concerns cases where contributions from two (or more) sources of uncertainty in the input variables have impact of similar magnitude on the output uncertainty. In such cases, the solution of the uncertainty allocation problem is non-unique, and the single-to-single workflow reversal setting is not adequate to handle the multiple combinations.

Recently, a methodology for uncertainty allocation has been proposed by Opgenoord and Willcox [14], which will be referred to here as the ‘resource allocation optimization method’. It incorporates a sensitivity-based method, surrogate modelling to alleviate the issue of expensive model evaluations, and a weighted-sum optimization approach to identify and select candidate uncertainty sources on which the reduction of uncertainty should be focused. In the resource allocation optimization method, only uniform probability distribution functions (PDFs) are considered for the uncertainty on the input variables. In Ref. [14], it was indicated that the extension of the resource allocation optimization method to include other distribution types is straightforward, although the resulting parameterization may have more degrees of freedom per input. One approach to set other types of input distributions is to consider all the statistical moments (e.g., first four moments), however, directly manipulating the statistical moments of the input distribution poses a problem of guaranteeing that the input PDFs can be reconstructed.

In this paper, we address these limitations by proposing a method intended to enhance the process of interactive uncertainty allocation. The aim is to enable the systematic investigation of tradeoff strategies regarding input-variability. The approach builds upon the ‘inverse uncertainty propagation’ method, introduced by Chen et al.[8]. The specific objectives of the work presented in this paper are to: a) Extend functionality, by introducing the ability to consider multiple outputs with multiple input reductions of uncertainty, by means of exploring the shapes of the parameterized distributions functions; b) Enable an interactive trade off process of multiple combinations of uncertainty allocation, by introducing visualization of the decision (trade) space; and c) combine (a) and (b) with an efficient uncertainty propagation method [15], to enable faster interactive uncertainty allocation.

The paper is organized as follows: the problem and background information are presented in Section 2. The proposed method is introduced in Section 3 and is demonstrated with an industrially relevant aircraft thermal system integration example in Section 4. The approach is evaluated by means of comparison against the state-of-the-art method in Section 5. Finally, conclusions are drawn and future work is outlined in Section 6.

2 PROBLEM STATEMENT

The problem addressed in this work is subject to the following definitions, scope, and assumptions:

- There are two major classes of uncertainty – aleatory and epistemic [16],[17]. Aleatory uncertainty is classed as irreducible, and includes, for example, operational variability. Epistemic uncertainty is also known as reducible or lack of knowledge. We consider only epistemic uncertainty, and this is modelled with probability distributions. The distributions can be considered as representations of ‘subjective beliefs’ of what the true values of the corresponding variables should be. For example, at the conceptual design stage, some material properties may be uncertain because the material itself has not yet been decided upon. Until all the relevant design studies have been conducted and a subsequent decision regarding the material to be used is made, the values for these properties cannot be fixed.
- Quantifying the sources of uncertainty in probabilistic terms requires (expert) elicitation at the outset [18]. However, this is out of the scope of this paper and it will be assumed as given.
- The input probability distributions are assumed independent.
- In order to calculate the probability of meeting a constraint, it is assumed that the output distributions are Gaussians. If one or all outputs are not Gaussian distributions, the method by Padulo and Guenov [19] can be employed to make assumptions on the type of output distribution, e.g., symmetric unimodal, or asymmetric unimodal output distribution. Alternatively, a study should be carried out to assess if the output can be approximated by another type of distribution that can be defined with the first two moments.

Under the above assumptions, a formal definition of the problem is stated as follows: consider reshaping the probability distribution by manipulating parameters, \mathbf{d}_x , of the input probability density function, f_x , such that the required constraints are met. This can be formulated as:

Given computational workflow, or model, $Y = h(X)$,

$$\begin{aligned} & \underset{d \in \mathcal{A}}{\text{find}} f_{x_i}(x_i, d_{x_i, p_i}), i = 1, \dots, I, \\ & \text{such that } g_j(X) \leq 0, j = 1, \dots, J, \end{aligned} \quad (1)$$

where $g_j(X)$ is the constraint function that can be recast as:

- 1) $g_j(X) = d_{y_j}(y_j(X)) - d'_j$, where d'_j is the constraint value on the parameters describing the variability on the j^{th} output of interest, e.g., tolerance constraint. These parameters could be functions of the statistical moments of the output probability density function, f_{y_j} .
- 2) $P(g_j(X) \leq 0) \geq P_{g_j}$, where P_{g_j} is the probability of satisfying the j^{th} constraint, $g_j(X) = y_j(X) - y'_j$; and y'_j is the quantile representing the constraint value of the j^{th} output of interest. Here, the variability is implicit in the probability of constraint satisfaction.

The problem is illustrated in Figure 1. Suppose that, after propagating the uncertainty forward, the designer realizes that the probability of meeting a constraint, $P(g_j(X) \leq 0)$, affected by uncertainty, y_{g_j} , is not satisfactory. One course of action is to investigate whether uncertainty in the inputs could be reduced. The problem is to decide where to allocate uncertainty affecting the input variables, X , for a pre-defined probability of constraint satisfaction, P_{g_j} .

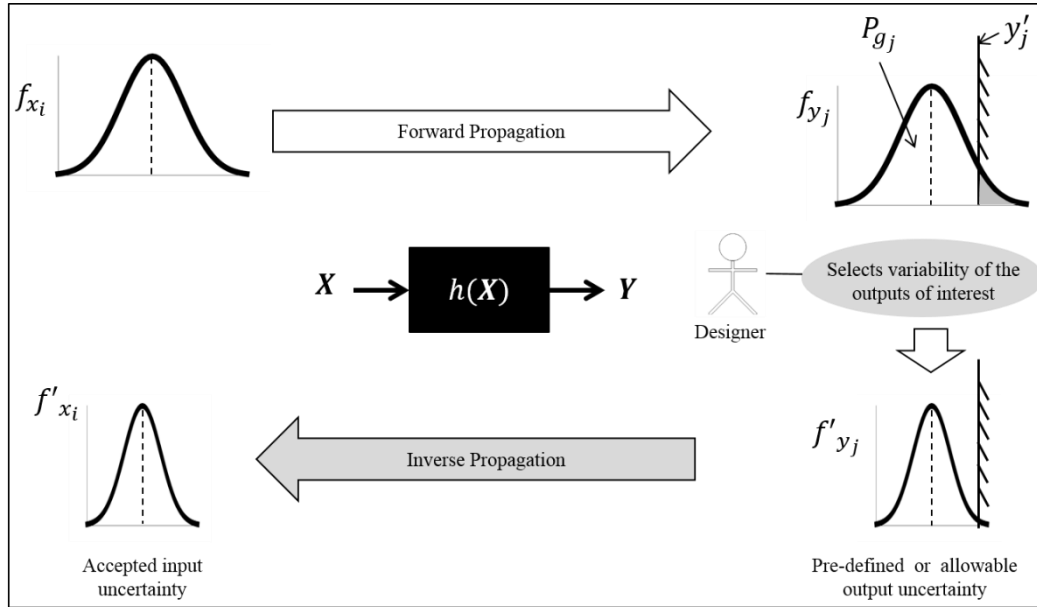


Figure 1. The process of allocating uncertainty.

2.1 ILLUSTRATIVE EXAMPLE

Consider a simple aircraft-sizing problem, using the Breguet range equation:

$$Range = V_{cruise} \left(\frac{L/D}{sfc} \right) \ln \left(\frac{W_{empty} + W_p + W_f}{W_{empty} + W_p} \right), \quad (2)$$

The definitions and values of the parameters in Eq. (2) are given in Table 1, along with the associated variability, where applicable. It is assumed that only the airframe empty weight (W_{empty}) and the propulsion performance (sfc) are affected by epistemic uncertainty.

The objective is to determine whether the requirement on $Range \geq 3000$ nm can be met with $\pm 5\%$ of variability in W_{empty} and sfc . This problem can be formulated as finding the PDFs of the input uncertainties, $f_{W_{empty}}(d_{W_{empty}})$ and $f_{sfc}(d_{sfc})$, by manipulating their distribution parameters, \mathbf{d} , such that the constraints are met. This can be stated mathematically as follows:

$$\begin{aligned} & \underset{\mathbf{d} \in \mathcal{A}}{\text{find}}(f_{W_{empty}}(d_{W_{empty}}), f_{sfc}(d_{sfc})), \\ & \text{such that } \begin{cases} P_{Rng}(Range(\mathbf{d}) \geq 3000nm) \geq 85\%, \\ \sigma_R(\mathbf{d}) \leq \sigma_{R,b}, \\ Cost(\mathbf{d}) \leq C_b, \end{cases} \end{aligned} \quad (3)$$

where,

$\mathbf{d} = (d_{W_{empty}}, d_{sfc})$ is the vector of two upper and lower bounds of the input variability, e.g., $d_{W_{empty}} = 5\%$.

$\sigma_{R,b}$ is the budget on the output uncertainty, in this case determined by the standard deviation, $\sigma_R(\mathbf{d})$, and

C_b is the cost budget on the $Cost(\mathbf{d})$.

Similar to Opgenoord and Willcox [14][20], the uncertainty and cost budgets in Eq.(3) have been included as constraints, such that the cost budget enforces limits on the resources that can be expended to reduce uncertainty. For simplicity the following linear cost model was utilized:

$$Cost = 10(10 - d_{W_{empty}} - d_{sfc}). \quad (4)$$

Table 1. Parameter values for the simple aircraft-sizing example

Parameter	Nominal value
V_{cruise}	450 kts
L/D	18.5
W_{empty}	82500 lbs
W_p	54000 lbs
W_f	37000 lbs
sfc	0.657 lb/h/lb

The uncertainties were modelled as two independent Gaussian distributions. The $\pm 5\%$ of variability can be fitted by truncating the Gaussian distribution at $\pm 3\sigma$. The means, $(\mu_{W_{empty}}, \mu_{sfc})$ were equated to the nominal value of the design parameter. The standard deviation is modelled as proportional to $\pm 5\%$ of variability, i.e., $\sigma = \pm 5\% \cdot (\mu/3)$, which results in $\sigma_{W_{empty}} = \pm 1375$ lb and $\sigma_{sfc} = \pm 0.01095$ lb/h/lb.

In order to determine the uncertainty in the range estimation, the forward propagation was conducted using Monte Carlo Simulations (MCS). The mean of *Range*, $\mu_R = 3041.38$ nm, and the standard deviation, $\sigma_R = 58.558$ nm, were used to calculate the probability to meet the requirement $P(Range \geq 3000nm)$. The result of this assessment shows that there is a 75.85% probability of constraint satisfaction for the range.

Next, it is assumed that the probability to meet the requirement is not acceptable. A course of action would be to investigate the combinations of input variability, i.e., to determine how much uncertainty in W_{empty} and sfc should be reduced to achieve 85% target probability of meeting the range constraint.

2.2 INDEPENDENT GAUSSIAN DISTRIBUTIONS TRANSFORMATION

Although stated in Section 2 that the input probability distributions are assumed independent, a transform into statistically independent distributions can be used. As proposed in Ref [21], for two joint Gaussian distributions with correlated coefficient ρ , statistically independence can be achieved by applying linear transformation or coordinate rotation. Considering the illustrative example, rewriting the general joint Gaussian distribution, $f(sfc, W_{empty})$, as the normalized distribution, $N(1,0)$, with $\alpha_1 = (sfc - \mu_{sfc})/\sigma_{sfc}$, $\alpha_2 = (W_{empty} - \mu_{W_{empty}})/\sigma_{W_{empty}}$, results in:

$$f_{\alpha}(\alpha_1, \alpha_2) = \frac{1}{2\pi\sqrt{1-\rho^2}} \exp\left\{-\frac{\alpha_1^2 - 2\rho\alpha_1\alpha_2 + \alpha_2^2}{2(1-\rho^2)}\right\}. \quad (5)$$

Applying the linear transformation $(\alpha_1, \alpha_2) \rightarrow (\beta_1, \beta_2)$, in which

$$\begin{aligned}\beta_1 &= \alpha_1 \cos(\pi/4) + \alpha_2 \sin(\pi/4), \\ \beta_2 &= -\alpha_1 \sin(\pi/4) + \alpha_2 \cos(\pi/4).\end{aligned}$$

The exponent of $f(\alpha_1, \alpha_2)$ simplifies to $\alpha_1^2 - 2\rho\alpha_1\alpha_2 + \alpha_2^2 = \beta_1^2(1 - \rho) + \beta_2^2(1 + \rho)$. Subsequently, Eq. (5) can be rewritten as the product of two distributions (Eq. (6)). They are therefore statistically independent and, by definition, uncorrelated.

$$f_\beta(\beta_1, \beta_2) = \frac{1}{\sqrt{2\pi(1+\rho)}} \exp\left\{-\frac{\beta_1^2}{2(1+\rho)}\right\} \cdot \frac{1}{\sqrt{2\pi(1-\rho)}} \exp\left\{-\frac{\beta_2^2}{2(1-\rho)}\right\}. \quad (6)$$

Eq. (6) can be rewritten as the non-normalized distribution with random variables, $sfc'(\beta_1)$ and $W'_{empty}(\beta_2)$, by substituting $\beta_1 = (sfc' - \mu_{sfc})/\sigma_{sfc}$ and $\beta_2 = (W'_{empty} - \mu_{W_{empty}})/\sigma_{W_{empty}}$ into Eq. (6), defining $\sigma'_{sfc} = \sigma_{sfc}\sqrt{1+\rho}$ and $\sigma'_{W_{empty}} = \sigma_{W_{empty}}\sqrt{1-\rho}$, and normalizing by $1/\sigma_{sfc}$ and $1/\sigma_{W_{empty}}$ respectively, results in two independent Gaussian distributions:

$$\begin{aligned}f'_{sfc} &= \frac{1}{\sigma_{sfc}} f_{\beta_1}(\beta_1) = \frac{1}{\sqrt{2\pi\sigma'^2_{sfc}}} \exp\left\{-\frac{(sfc' - \mu_{sfc})^2}{2\sigma'^2_{sfc}}\right\}, \\ f'_{W_{empty}} &= \frac{1}{\sigma_{W_{empty}}} f_{\beta_2}(\beta_2) = \frac{1}{\sqrt{2\pi\sigma'^2_{W_{empty}}}} \exp\left\{-\frac{(W'_{empty} - \mu_{W_{empty}})^2}{2\sigma'^2_{W_{empty}}}\right\}.\end{aligned} \quad (7)$$

Finally, if the correlated coefficient is $\rho=0.5$, the standard deviation of the independent Gaussian distribution result in $\sigma'_{W_{empty}}=\pm 972.27$ lb and $\sigma'_{sfc}=\pm 0.0134$ lb/h/lb. Percentage wise, these standard deviations correspond to $\pm 3.54\%$ and $\pm 6.12\%$ variability in W_{empty} and sfc respectively. The rest of the analysis can be carried out in the transformed space, $sfc'(\beta_1)$ and $W'_{empty}(\beta_2)$. Note that, for the remainder of the paper, the input probability distributions are assumed independent.

3 PROPOSED METHOD FOR ALLOCATING UNCERTAINTY AND TRADEOFF STRATEGY

As stated in the introduction, the aim of this work is to enhance the process of interactive uncertainty allocation, including the systematic investigation of tradeoff strategies regarding input-variability.

The intended novelty of the proposed approach, compared with the state-of-the-art methods [8],[14], is twofold:

a) the introduction of parameterization of the input distributions which allows varying all first four statistical moments, and

b) efficient visualization of the entire trade space, as opposed to only ‘optimal’ solutions. This enables the interactive exploration of the reversal of multiple outputs with multiple uncertainty input reductions.

In mathematical terms, the proposed method is concerned with the problem described by Eq. (1). The method consists of four steps:

3.1 IDENTIFICATION OF MAJOR CONTRIBUTING SOURCES OF UNCERTAINTY

As in the method by Chen et al. [8], the aim of this step is to identify the major contributing sources of input uncertainty that impact the output variables of interest. Applying a global sensitivity analysis can aid the designer to decide on which input variables efforts for reducing uncertainty should be focused. Once the major contributing sources of input uncertainty have been identified, their PDFs can be parameterized, as described next.

3.2 PARAMETERIZATION OF THE INPUT PROBABILITY DENSITY FUNCTIONS

One approach to find a suitable set of solutions that solve the problem described in Eq. (1), is to manipulate the statistical moments of the input PDFs, $f_{x_i}(x_i, d_{x_i, p_i})$, until all the probability of constraints satisfaction are met. In other words, the standard deviation could be reduced and/or the mean could be shifted and the same for the other moments, such as the skewness and kurtosis. Formulating the problem of finding multiple possible reductions of uncertainty, by directly manipulating the statistical moments of all input PDFs poses the problem of guaranteeing that the input PDFs are realizable (not all combinations of moments can represent a PDF). To address this, we propose parameterizing the function that defines the shape of the PDFs, by linking the first fourth statistical moments ($\mu_x, \sigma_x, \gamma_x, \Gamma_x$) of a particular PDF with, if possible, a single parameter, d_x . The parameterization must consider the fundamental properties of a PDF. The first property is that the density function be nonnegative ($f_{x_i}(x_i, d_{x_i}) \geq 0$) for all x_i , whereas the second property is that a PDF has to have an area of unity (i.e. $\int f_{x_i}(x_i, d_{x_i}) dx_i = 1$).

However, the statistical moments might not have explicit definition in terms of ‘engineering’ quantities. Here, the parameterization aims at manipulating the shape of the PDF with variables that design practitioners are familiar with, such as the lower and upper bounds that define the range of variation (x_{lb_i} and x_{ub_i}). Also, the variations are often described as a percentage of the nominal value, x_{n_i} . For example, considering the illustrative example in Section 2.1, the shapes of the Gaussian distributions, $f_{Wempty}(d_{Wempty})$ and $f_{Sfc}(d_{Sfc})$, can be parameterized with respect to the width of the distribution (i.e., lower and upper bounds). Subsequently, the width parameter can be related to the statistical

moments of the Gaussian distribution. It is assumed that the nominal value should not be changed, therefore the means of the Gaussians are equated to the nominal values. The standard deviations can be modelled as proportional to the upper and lower bounds of the variability, i.e., $\sigma_{W_{empty}} = d_{W_{empty}} \mu_{W_{empty}} / 3$ and $\sigma_{sfc} = d_{sfc} \mu_{sfc} / 3$. Here, we specifically introduce a parameterization for two types of PDF, namely triangular and Gaussian mixture, although this parameterization is not limited to these two.

3.2.1 Parameterization for triangular distributions

The triangular PDF $f_t(x)$ is defined with the bounds (x_{lb} and x_{ub}) and the mode at x_n , as shown in Figure 2a. The parameterization is defined using the width ($d_x = x_{ub} - x_{lb}$) of the distribution. The PDF can then be re-shaped by scaling the width with respect to the nominal value, x_n . For a new width, d'_x , the new parameters of the PDF are calculated with geometrical proportions and the unity area property of the triangle. The corresponding widths, the distance between x_n and the new bounds have lengths of the same ratio, as follows:

$$\begin{aligned} \frac{d'_x}{d_x} &= \frac{(x_n - x'_{lb})}{(x_n - x_{lb})}; \\ \frac{d'_x}{d_x} &= \frac{(x_n - x'_{ub})}{(x_n - x_{ub})}. \end{aligned} \quad (8)$$

The new bounds x'_{lb} and x'_{ub} can therefore be obtained from Eq. (8). After the new shape of the PDFs is defined, its first four moments are calculated:

$$\begin{aligned} \mu'_x &= \frac{(x_n + x'_{ub} + x'_{lb})}{3}; \\ var'_x &= \frac{(x'_{ub} - x'_{lb})^2}{18} \left(1 - \frac{(x_n - x'_{lb})(x'_{ub} - x_n)}{(x'_{ub} - x'_{lb})^2} \right); \\ \gamma'_x &= \frac{\sqrt{2}(x'_{lb} + x'_{ub} - 2x_n)(2x'_{lb} - x'_{ub} - x_n)(x'_{lb} - 2x'_{ub} + x_n)}{5((x'_{lb})^2 + (x'_{ub})^2 + x_n^2 - x'_{lb}x'_{ub} - x'_{lb}x_n - x'_{ub}x_n)^{3/2}}. \end{aligned} \quad (9)$$

The excess kurtosis, $\Gamma_x = -\frac{3}{5}$, remains invariant for a triangular PDF. Parameterization of uncertainty reduction can also be achieved by simply modifying either x_{ub} or/and x_{lb} with respect to x_n , thereby reducing the width.

Note that, the set of all possible shapes of the triangular distributions can be explored by varying independently, x_{lb} , x_{ub} , and x_n . In this case, the parameterization linked three statistical moments with a single parameter. However, this reduction in the degrees of freedom comes at the expense of reducing the space of all possible shapes of the triangular distribution.

3.2.2 Parameterization for Gaussian mixture distributions

In Figure 2b, the Gaussian mixture probability distribution [22], f_{gm} , is defined by two component functions with variances (σ_1^2 and σ_2^2) and means (μ_1 and μ_2), with proportions (α_1 and $\alpha_2 = 1 - \alpha_1$), so that

$$f_{gm}(x) = \alpha_1 \phi(x; \mu_1, \sigma_1^2) + \alpha_2 \phi(x; \mu_2, \sigma_2^2), \quad (10)$$

where $\phi(x; \mu, \sigma^2)$ denotes the univariate Gaussian PDF. The range of variability can be fitted by truncating ϕ at 3σ . The means can then be defined as: $\mu_1 = x_{lb} + 3\sigma_1$ and $\mu_2 = x_{ub} - 3\sigma_2$ (assuming $\mu_1 < \mu_2$); the standard deviations by $\sigma_1 = \sigma_2 = \frac{x_{ub} - x_{lb}}{8}$; the proportions by $\alpha_1 = \frac{|\mu_{x_0} - \mu_2|}{\mu_2 - \mu_1}$; whereas the mean, μ_{x_0} , of the Gaussian mixture PDF coincides with the nominal value, x_n . f_{gm} is left-skewed, if $x_n > \frac{x_{ub} + x_{lb}}{2}$, otherwise is right-skewed. Other Gaussian mixture parametric models can be found in McLachlan and Peel [21].

It is suggested that the Gaussian mixture PDF be parameterized in such a way that the skewness of the PDF can be manipulated by changing the position of the mean, μ_{x_0} . For example, it might be desirable to change the shape of f_{gm} from left-skewed (with mean $\mu_{x_0} = \mu_{x_l}$) to right-skewed (with mean μ_{x_r}), as shown in Figure 2b. This can be achieved by switching the proportions of f_{gm} the skewness changes from being left-skewed to right-skewed, where the respective means are given by

$$\begin{aligned} \mu_{x_l} &= \alpha_1 \mu_1 + \alpha_2 \mu_2; \\ \mu_{x_r} &= \alpha_2 \mu_1 + \alpha_1 \mu_2. \end{aligned} \quad (11)$$

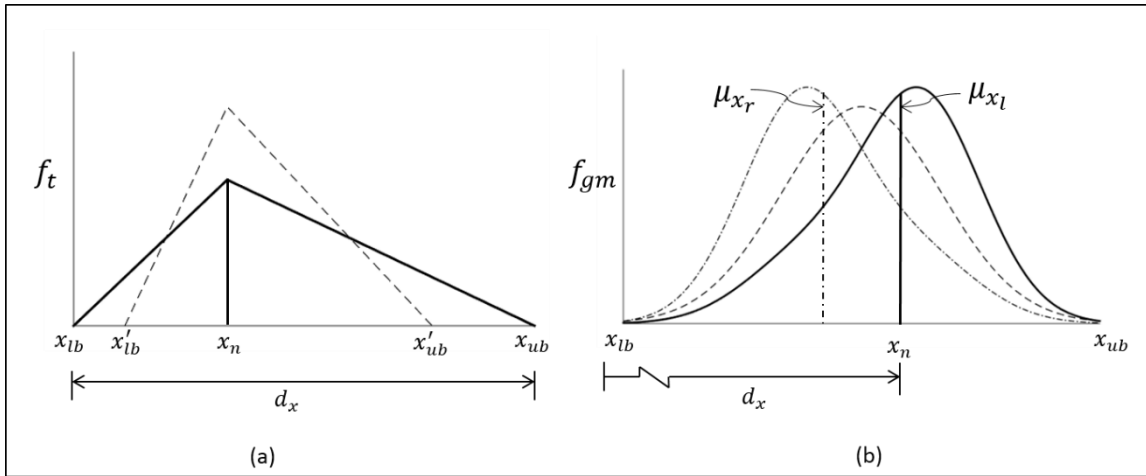


Figure 2. Parameterization of the input probability density function, a) triangular distribution and b) Gaussian mixture distribution.

For the shapes, in between the left- and right-skewed distributions (for example, a symmetric distribution), f_{gm} can be re-shaped by defining the nominal value, $x_n = d_x$, as input parameter, μ'_x (which is bound in the range $\mu'_x \in [\mu_{x_r}, \mu_{x_l}]$). The parameterization involves the linear transformation of component functions of Eq. (10) (i.e. new means, μ'_1, μ'_2 , and new standard deviations, σ'_1, σ'_2) by making changes to the position, μ'_x , as follows:

$$\begin{aligned}\mu'_1 &= \mu_1 + \Delta\mu; & \mu'_2 &= \mu_2 - \Delta\mu; \\ \sigma'_1 &= \frac{(\mu'_1 - x_{lb})}{3}; & \sigma'_2 &= \frac{(x_{ub} - \mu'_2)}{3},\end{aligned}\tag{12}$$

where $\Delta\mu$ is given by:

$$\Delta\mu = \begin{cases} (\mu_2 - \mu_1) \left(\frac{\mu_{x_l} - \mu'_x}{\mu_{x_l} - \mu_{x_r}} \right); & \alpha_1 = \frac{|\mu_{x_l} - \mu_2|}{\mu_2 - \mu_1}; \alpha_2 = 1 - \alpha_1; \text{ if } \mu'_x > \mu_{x_r} + \frac{(\mu_{x_l} - \mu_{x_r})}{2} \\ (\mu_2 - \mu_1) \left(\frac{\mu'_x - \mu_{x_r}}{\mu_{x_l} - \mu_{x_r}} \right); & \alpha_2 = \frac{|\mu_{x_l} - \mu_2|}{\mu_2 - \mu_1}; \alpha_1 = 1 - \alpha_2; \text{ otherwise.} \end{cases}\tag{13}$$

where μ_{x_l} and μ_{x_r} are given in Eq. (11). As mentioned before in the parameterization of the triangular PDF, after the new shape of the PDFs is defined, its first four moments are calculated and used for uncertainty propagation methods. Calculating the first four moments of a Gaussian mixture is well understood and can be found in McLachlan and Peel [21].

3.3 WORKFLOW COMPOSITION FOR UNCERTAINTY ALLOCATION

The objective of this step is to create a workflow that enables inverse uncertainty propagation (see Figure 1) by means of reversing the default workflow. Reversal refers to the capability of ‘swapping’ input and output variables of a computational workflow. In this work, the workflow reversal is based on a computational workflow management (CWM) method, developed by Balachandran and Guenov [23]. The CWM method enables the automatic formulation of the reversed workflow into an optimization problem, which is solved using optimization algorithms (e.g., Gauss-Newton, or fixed-point iteration). This capability allows the investigation of ‘what-if’ scenarios and conducting flexible computational studies.

It was demonstrated by Chen et al.[8] that the standard deviation of an input variable of a default workflow (original sequencing) can be swapped with one of the standard deviations of the original output variables. However, this approach can only be applied to input distributions with only one statistical moment as a degree of freedom. The parameterization presented in Section 3.2 overcomes this limitation and enables the exploration of shapes of the parameterized distributions functions by varying more than one statistical moment.

Consider the illustrative example in Section 2.1 and Figure 3. The workflow is created in the following sequence:

- 1) An outer workflow [8] is created to associate the statistical moments ($\sigma_{W_{empty}}$, $\mu_{W_{empty}}$, σ_{sfc} , μ_{sfc} , μ_R , and σ_R , the skewness, γ_X , and kurtosis, Γ_X remain constant) with the inputs and two moments of the output variables of the Breguet equation Eq.(2). (refer to the center of Figure 3).
- 2) The parameterization ($d_{W_{empty}}$ and d_{sfc}) of the Gaussian distributions (left of Figure 3) and the probability of constraint satisfaction of the parameter *Range* are linked to the 'outer workflow'.

The result is a global workflow which links parameters $d_{W_{empty}}$ and d_{sfc} of the parameterized PDFs to the probability of constraint satisfactions of the outputs of interest. Subsequently, in order to compute how much uncertainty can be accepted from the inputs, the reversed workflow could be used. A possible scenario could be to swap the input variability on propulsion performance, d_{sfc} , with the output variable related to the probability of constraint satisfaction of P_{Rng} , which is indicated by the dotted arrows in Figure 3.

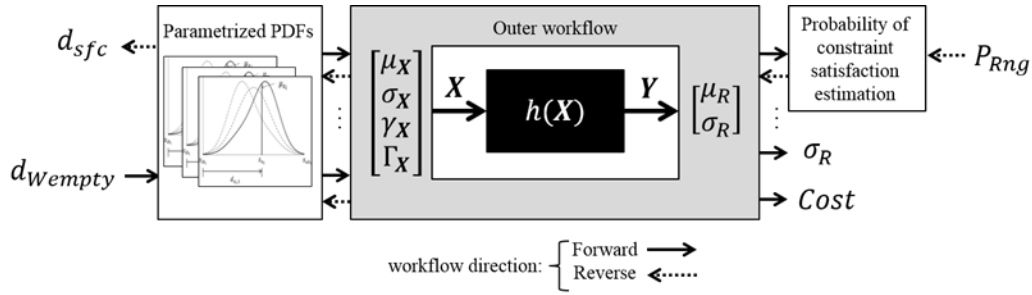


Figure 3. Global workflow creation.

Once established, the workflow reversal can be used to generate a particular solution. However, often the contributions from two (or more) sources of uncertainty in the input variables could have impact of similar magnitude on the output uncertainty. In this case, the solution will have multiple combinations of reduced distributions. In other words, the solution of the uncertainty allocation problem is non-unique, and the workflow reversal setting is not fully adequate to handle multiple combinations. This issue can be explored by means of visualization of the multiple combinations as proposed in the next section.

3.4 TRADEOFF SPACE VISUALIZATION

The objective of this step is to visualize the multiple combinations in a trade space. The tradeoff space can be visualized with 2-d 'slices' (2-dimensional cross-sectional plots) of the trade space. Although the illustrative example involves two-dimensional trade spaces, this technique can be applied to a multi-dimensional trade space in the following way:

1. The n -dimensional input space can be broken into parameter pairs, e.g., (x_1, x_2) , (x_3, x_4) , ..., (x_{n-1}, x_n) . All n parameters should be visualised in pairs. In the case of odd numbers, one of the parameters can be repeated.
2. Each pair will represent a plane (slice) of the hyper-cube. The planes are intersected at a point of interest (e.g., nominal value).

3. The m -dimensional output space can be visualized with two-dimensional cross-sections of the space that contain iso-contours representing the constraints (which are either deterministic or probabilistic). There is, in essence, no limit on the number of contours that could be considered but trying to compute and visualize too many could prove impractical. The aim of computing the contours is to identify feasible regions encompassed by them. This is done by computing and drawing the iso-contours corresponding to a particular value of the probability of constraint satisfaction. Considering the illustrative example in Section 2.1, the generalized isocontour-based constraint analysis method [24], was employed to visualize all possible combinations that could lead to 85% of probability of meeting the 3000 nm range constraint. The workflow was employed to compute the full factorial sampling of the discretized design space, which was carried out in the following manner: $d_{W_{empty}} \times d_{sfc} = \{0, 1.25, 2.5, 3.75, 5\} \% \times \{0, 1.25, 2.5, 3.75, 5\} \%$.
4. The exploration can take place by moving the intersection point to visualize other planes.

Scaling to higher input (and output) dimensions increases the number of possible planes or slices, and thus the complexity of the analysis. However, this approach could immediately provide information about the possible action to be taken, depending on the local behavior of the constraints in the design space. This is demonstrated in the industrial example (Section 4).

Regarding the illustrative example, the trade space is presented in Figure 4 where the green dots represent sampled points. The designer can select the value of the constraint, for example, to visualize the feasible region associated with Eq. (3). In this case, the feasible region was determined by setting P_{Rng} to 85%, the uncertainty budget, $\sigma_{R,b}$, to 40lb and the cost budget, C_b , to 40. In Figure 4a, the feasible region is represented by the area colored in white. Note that the constraint σ_R is inactive. The exploration of possible options for allocating uncertainty can now be sought, for example, some solutions along the active constraint, P_{Rng} , marked as 'A', 'B' and 'C'. Solution 'A' is one in which only the uncertainty in the sfc should be reduced (to almost 50% of its original value). Solutions 'B' or 'C' constitute compromises, in which uncertainty should be reduced in both sfc and airframe empty weight.

Other scenarios can be easily be explored. For example, P_{Rng} could be set to, say, 95% for the probability of constraint satisfaction, and the cost budget, C_b , relaxed, by increasing it to 70. The new tradeoff space associated with such changes can then be revisualized (see Figure 4b) without extra computational workflow executions. Similarly, further combinations of possible options for allocating uncertainty can be sought in Figure 4b.

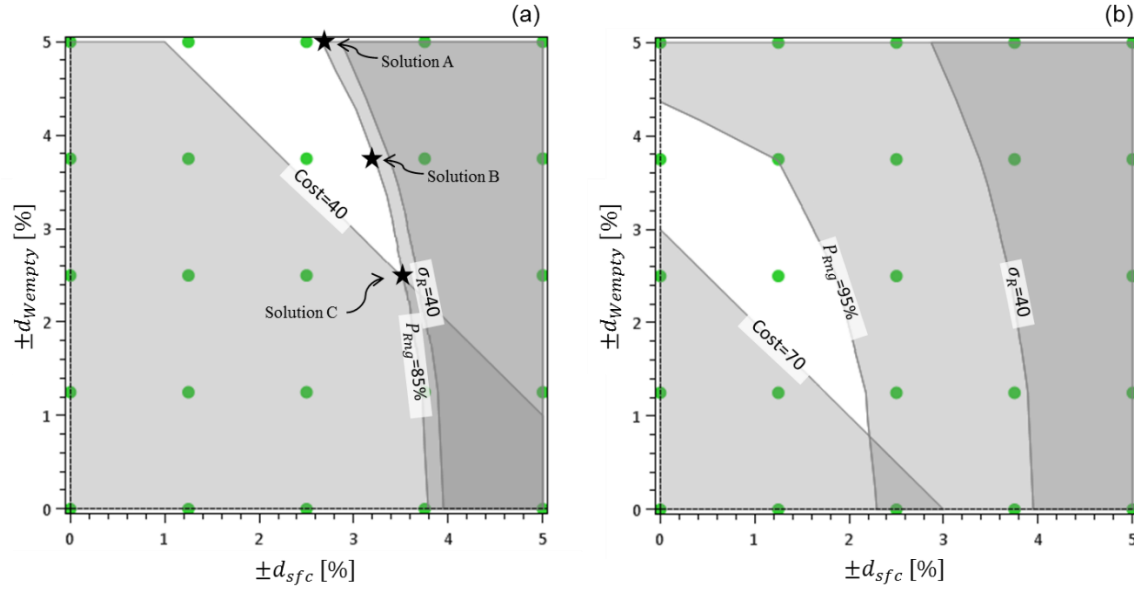


Figure 4. The tradeoff space of the illustrative example.

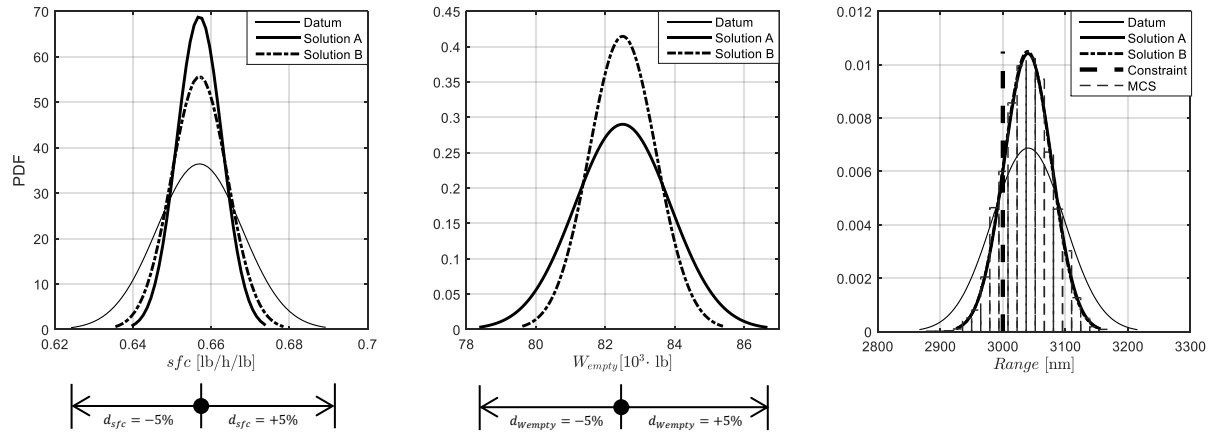


Figure 5. Results of uncertainty allocation in the illustrative example.

Once the iso-contours have been generated, the workflow reversal can be utilized to obtain improved estimates of the numerical values for solutions, such as ‘A’, ‘B’ and ‘C’ in Figure 4a. Specifically, the input variability on propulsion performance, d_{sfc} , is swapped with the probability of constraint satisfaction of P_{Rng} . The numerical results for ‘A’ to ‘C’ are presented in Table 2 and the corresponding input and output PDFs of ‘A’ and ‘B’ are presented in Figure 5. The uncertainty propagation was conducted using the fast propagation Univariate Reduced Quadrature (URQ) [15] method. The URQ method is a suitable choice because it can be used in combination with the parameterization proposed in Section 3.2, i.e., it employs the first four statistical moments of the uncertainty sources as input. MCS was also used to confirm that the output distribution can be approximated as a Gaussian. In addition, the Kolmogorov-Smirnov test has

been carried out on the output distributions for the datum and solutions, and the numerical results returned show that the data generated with MCS comes from a standard normal distribution.

Table 2. Comparison of the input variability before and after uncertainty allocation.

Allocations	Input variable reversed d_{sfc}	Input variable d_{wempty}	Probability of constraint Satisfaction		
			P_{Rng}	$\sigma_R[nm]$	$Cost$
Datum	$\pm 5\%$	$\pm 5\%$	75.85%	57.558	0
Solution A	$\pm 2.646\%$ ^a	$\pm 5\%$	85% ^b	38.215	23.540
Solution B	$\pm 3.274\%$ ^a	$\pm 3.5\%$	85% ^b	38.266	32.260
Solution C	$\pm 3.527\%$ ^a	$\pm 2.5\%$	85% ^b	38.254	39.730

^aOutput value calculated with the workflow reversal, ^bPre-defined, input value to the workflow reversal.

4 INDUSTRIAL EXAMPLE: AIRCRAFT THERMAL INTEGRATION DESIGN

To demonstrate how the method can handle more complex parameterization of the input probability distribution functions, it was applied to a representative industrial problem concerning avionics thermal integration of a single-aisle aircraft [3]. It is assumed that the design variables are affected by epistemic uncertainty and its impact needs to be assessed.

4.1 PROBLEM SPECIFICATION

The thermal performance of the avionics equipment was computed with a surrogate model of the Zonal Thermal Model (ZTM; model provided by M. Cappitelli, F. Mangeant, and M. Fouquembergh, TOICA Partners from Airbus Group Innovations, Feb. 2016) which has five input variables and 69 output variables. For illustration purposes, we considered three outputs of interest, with the following respective thermal constraint (requirements):

- Total mean temperature, over all equipment surfaces: $Temp_{total} \leq 325.15 \text{ K (52}^\circ\text{C)}$
- Maximum surface temperature of the power center: $Temp_{PC} \leq 319.15 \text{ K (46}^\circ\text{C)}$
- Maximum surface temperature of the battery: $Temp_{BAT} \leq 324.15 \text{ K (51}^\circ\text{C)}$

Uncertainty quantification was applied, under the following assumptions:

- Each uncertainty input could be modelled in the form of an independent probability distribution function (e.g. a triangular or Gaussian mixture distribution, as was shown in Figure 2). The parameters of the probability distributions were based on expert opinions from practicing designers in the TOICA project. The detailed specification for the problem is shown in Table 3.

- Variability in the inputs was considered to be the main source of uncertainty, whereas model uncertainty (simulation errors) was assumed to be negligible (in comparison with the sources of uncertainty listed in Table 3).

Table 3. Sources of uncertainty for the ZTM use case (data provided by M. Cappitelli, F. Mangeant, TOICA Partners from Airbus Group Innovations, Feb. 2016).

No .	Input variable	Nominal value and range of variability	Description of uncertainty	Probability distribution function
1	\dot{m}_{PC}	0.0274 kg/s; [0.0232, 0.0348]	Range of fluctuations	Rayleigh, $f_{\dot{m}_{PC}} = \frac{2}{b}(\dot{m}_{PC} - a)e^{-\frac{(\dot{m}_{PC}-a)^2}{b}}$ $a=0.0232, b = 2\left(\frac{0.0348-a}{3.5}\right)^{2.5}$
2	$Temp_{Fus}$	$-8^{\circ}\text{C} \pm 5^{\circ}\text{C}$	Lack of definition (i.e. epistemic)	Gaussian, $f_{Temp_{Fus}}$ $\mu=-8^{\circ}\text{C}, \sigma=5/3^{\circ}\text{C}$
3	HTC	1; -50%,+100%	Lack of definition (e.g. the material hasn't been selected yet)	Triangular, f_{HTC} $x_{lb}=0.5, x_{ub}=2, x_n=1$
4	$Heat_{diss}$	105 W/m ² ; [85, 120]	Range of fluctuations of dissipated power	Normal Mixture, $f_{Heat_{diss}}$ $\mu_1=785/8 \text{ W/m}^2, \sigma_1=35/8 \text{ W/m}^2$ $\mu_2=855/8 \text{ W/m}^2, \sigma_2=\sigma_1$
5	$Temp_{NLG}$	$10^{\circ}\text{C} \pm 5^{\circ}\text{C}$	Lack of definition (i.e. epistemic)	Gaussian, $f_{Temp_{NLG}}$ $\mu=10^{\circ}\text{C}, \sigma=5/3^{\circ}\text{C}$

The forward propagation was conducted by means of the URQ method, which returns the mean and standard deviation of all output variables of interest. The numerical results are reported in Figure 6. As can be seen in Figure 6, five thousand MCS points are sufficient to reach a 95% confidence level on the estimate of the constraint satisfaction probability. Also, the MCS results can be approximated by Gaussian distributions. This is confirmed by plotting a Gaussian PDF in Figure 6 (output distributions), using the mean and standard deviation from the URQ forward propagation.

The result of this assessment confirmed that the probability of constraint satisfaction ($P_{Temp_{total}}=74.78\%$, $P_{Temp_{PC}}=67.99\%$, and $P_{Temp_{BAT}}=60.15\%$) was not sufficient and it was required to be increased (to 95%). This problem could subsequently be formulated as an uncertainty allocation problem. The objective was therefore to find the parameters, \mathbf{d}_x , of the marginal probability distributions (see Table 3) that reduce the input uncertainty such that the probability to meet the thermal constraints of the avionics equipment is equal or greater to the requested probability of 95%. This can be stated mathematically as follows:

$$find(f'_{\dot{m}_{PC}}(\mathbf{d}_1), f'_{Temp_{Fus}}(\mathbf{d}_2), f'_{HTC}(\mathbf{d}_3), f'_{Heat_{diss}}(\mathbf{d}_4), f'_{Temp_{NLG}}(\mathbf{d}_5))$$

$$such\ that \begin{cases} P(Temp_{total} \leq 325.15\ K) \geq 95\% \\ P(Temp_{PC} \leq 319.15\ K) \geq 95\% \\ P(Temp_{BAT} \leq 324.15\ K) \geq 95\% \end{cases} \quad (14)$$

To this end, we have the scenario depicted in Figure 1 and the proposed method can be applied, as described next.

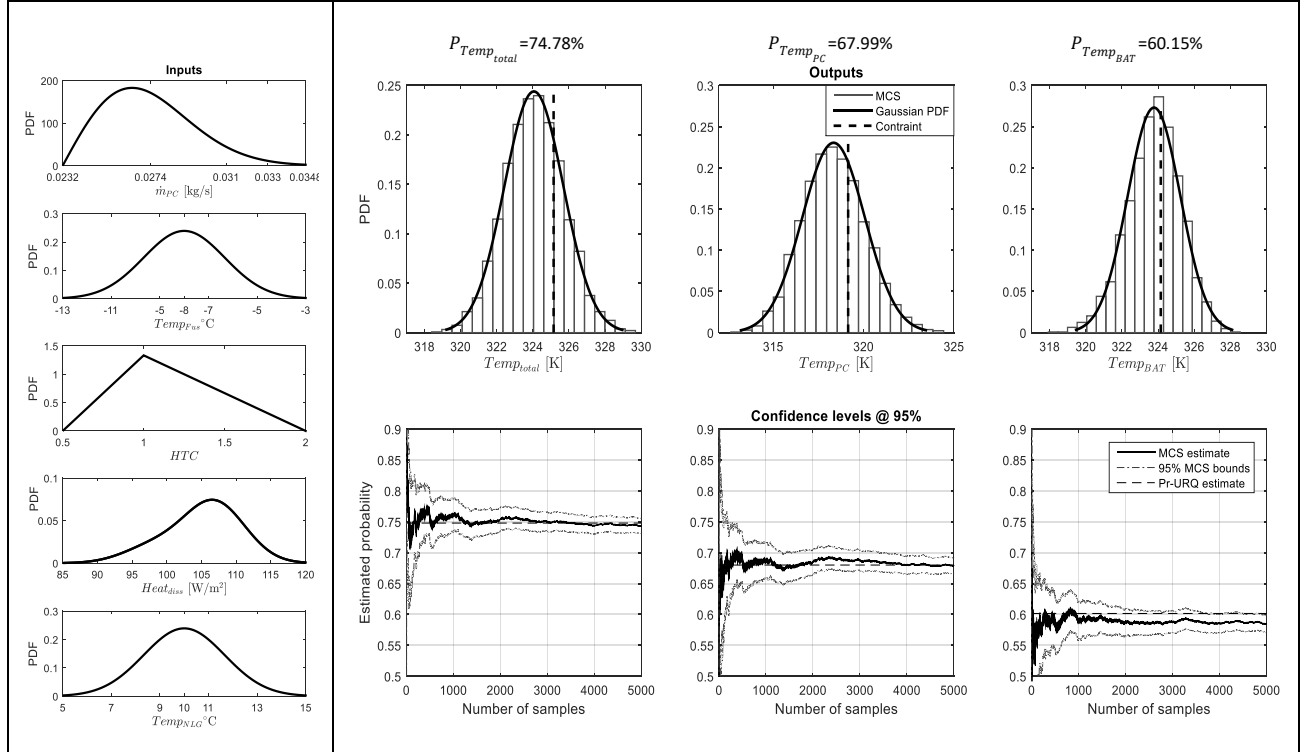


Figure 6. Forward propagation of uncertainty in the ZTM use case.

4.2 IDENTIFICATION OF MAJOR UNCERTAINTY CONTRIBUTORS FOR THE ZTM USE CASE

The aim of this step is to determine which sources of uncertainty have contributed the most to the variation in the output. A sensitivity analysis method, known as Fourier Amplitude Sensitivity Test (FAST) [25] was employed. The results in Figure 7 show that, among all the inputs with uncertainty, HTC and $Heat_{diss}$ were the main contributors and it was decided that they had to be reduced.

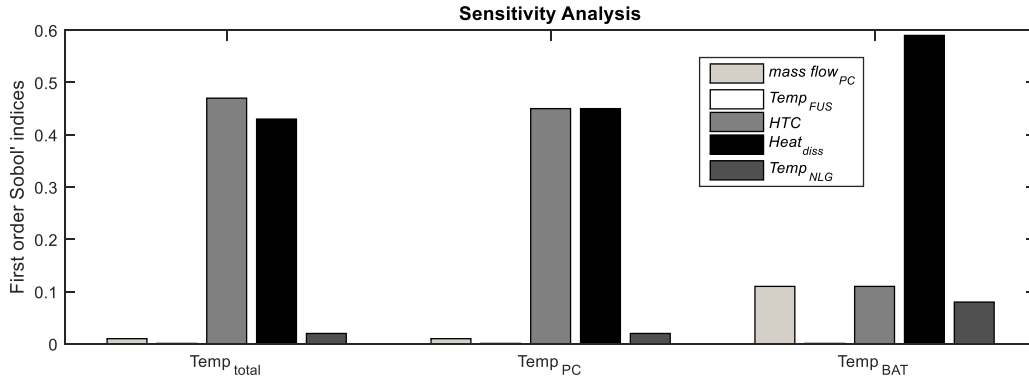


Figure 7. Sensitivity analysis results to identify contributions from different sources of uncertainty of the ZTM use case.

4.3 UNCERTAINTY PARAMETERIZATION OF PDFS OF THE ZTM USE CASE

The parameterization of the triangular distribution, f_{HTC} , and the Gaussian mixture PDFs, $f_{Heat_{diss}}$, was then performed as described in step two of Section 3. The shape of f_{HTC} was parameterized with respect to the base, or width, of the triangular distribution. Because high values of thermal material properties defined by HTC are desirable, only the variability on the left-hand side of the nominal value was reduced. The parameter used for uncertainty reduction was d_{HTC} . The shape of $f_{Heat_{diss}}$ was parameterized in two ways: first, the skewness was parameterized as illustrated in Figure 2b, where the parameter used for uncertainty reduction was $d_{Heat_{diss},\mu}$ of the Gaussian mixture PDF. The second way to reduce uncertainty was using the width, $d_{Heat_{diss},w}$, of the PDF, where the parameterization employed was the same as the triangular PDF illustrated in Figure 2a. A summary of the PDF parameter vector $\mathbf{d} = (d_{HTC}, d_{Heat_{diss},\mu}, d_{Heat_{diss},w})$ and its relation to the trade space is shown in Table 4.

Table 4. Specification of parameters of f_{HTC} and $f_{Heat_{diss}}$.

PDF & parameters relation	Parameter vector, $\mathbf{d} \in A$
$x'_{lb} = x_{ub} - d_{HTC}$	$d_{HTC} \in \{1, 1.125, 1.25, 1.375, 1.5\}$
$d_{Heat_{diss},\mu} = \mu'_x$	$d_{Heat_{diss},\mu} \in \{100, 101.25, 102.5, 103.75, 105\};$ [W/m ²]
$d_{Heat_{diss},w} = x'_{ub} - x'_{lb}$	$d_{Heat_{diss},w} \in \{5, 12.5, 20, 27.5, 35\};$ [W/m ²]

4.4 CREATING THE WORKFLOW FOR THE THERMAL INTEGRATION PROBLEM

As described in Section 3.3 and in similar fashion as depicted in Figure 3, an ‘outer workflow’ of the ZTM was created to associate the statistical moments with the input and output variables of the model. These moments were further reformulated with parameterization of the f_{HTC} and $f_{Heat_{diss}}$ PDFs. The parameterization models, the outer workflow and the probability of constraint satisfaction model of the outputs of interest ($P_{Temp_{total}}$, $P_{Temp_{PC}}$, and $P_{Temp_{BAT}}$) constituted the entire workflow. Therefore, the user could specify the parametric variables d_{HTC} , $d_{Heat_{diss},\mu}$, and $d_{Heat_{diss},w}$ and then obtain the probability of output constraint satisfaction (indicated by the black arrows in Figure 3). Subsequently, employing the workflow reversal method, the probability of output constraint satisfaction can be specified as a target. The execution of a reversed workflow could then be used to compute how much uncertainty can be accepted from the respective inputs (i.e. the parameterized input PDFs) to achieve the target probability. Here, two possible workflow reversal cases could be set up:

- 1) Reversal of the input variable related to the width, d_{HTC} , of the HTC PDF, with the output variable related to the probability of constraint satisfaction $P_{Temp_{PC}}$, while selecting the value of the parameters, $d_{Heat_{diss},\mu}$ and $d_{Heat_{diss},w}$, of the heat dissipation PDF (input).
- 2) Reversal of the input variable related to the skewness $d_{Heat_{diss},\mu}$ of the heat dissipation PDF, with the output variable related to the probability of constraint satisfaction of $P_{Temp_{BAT}}$, while selecting the value of the input parameters, $d_{Heat_{diss},w}$ and d_{HTC} .

As the solution to the uncertainty allocation problem is non-unique, several combinations of values for the parametric variables could potentially lead to 95% probability of constraint satisfaction. The next step is to visualize all these combinations.

4.5 TRADE SPACE VISUALIZATION OF THE ZTM USE CASE

As described earlier, the proposed approach enables the visualization of multiple possible combinations of reduction in uncertainty and supports interactive decision-making regarding the allocation of uncertainty. Following the steps proposed in Section 3.4, the three-dimensional tradeoff space can be visualized with 2-d slices (2-dimensional plots) as follows:

1. The 3-dimensional input space can be represented by means of two perpendicular slices form with the two variable pairs, $(d_{Heat_{diss},\mu}, d_{HTC})$ and $(d_{Heat_{diss},w}, d_{HTC})$.
2. The generalized isocontour-based constraint method [24] is then employed. In this case, a full factorial sampling of the design space is specified by discretizing the PDF parameters into five levels each, as shown in Table 4. Figure 8d illustrates two intersection points. The one marked with a triangle shows the intersection of the two planes, whereas the other intersection, marked with a large dot $(d_{HTC}, d_{Heat_{diss},\mu}, d_{Heat_{diss},w}) = (1, 105, 5)$ is at one of the corners of the 3-dimensional cube (trade space). The dot represents the nominal intersection and the intersecting planes at this point can be seen in Figure 8a-c. Note that two slices are sufficient for visualization of the input parameters (three in this case).

3. In Figure 8a-b, the output space is visualized with three probabilities of constraint satisfaction as iso-contours. One of the slices shows the feasible region in white, where the probability of satisfaction is higher than 95% for all the three outputs of interest, while the grey areas are infeasible. Exploration of the trade space shows that $P_{Temp_{total}} = 95\%$ is an inactive constraint, whereas the $P_{Temp_{PC}}$ and $P_{Temp_{BAT}}$ contours at 95% are active constraints and form a 'Pareto front'.

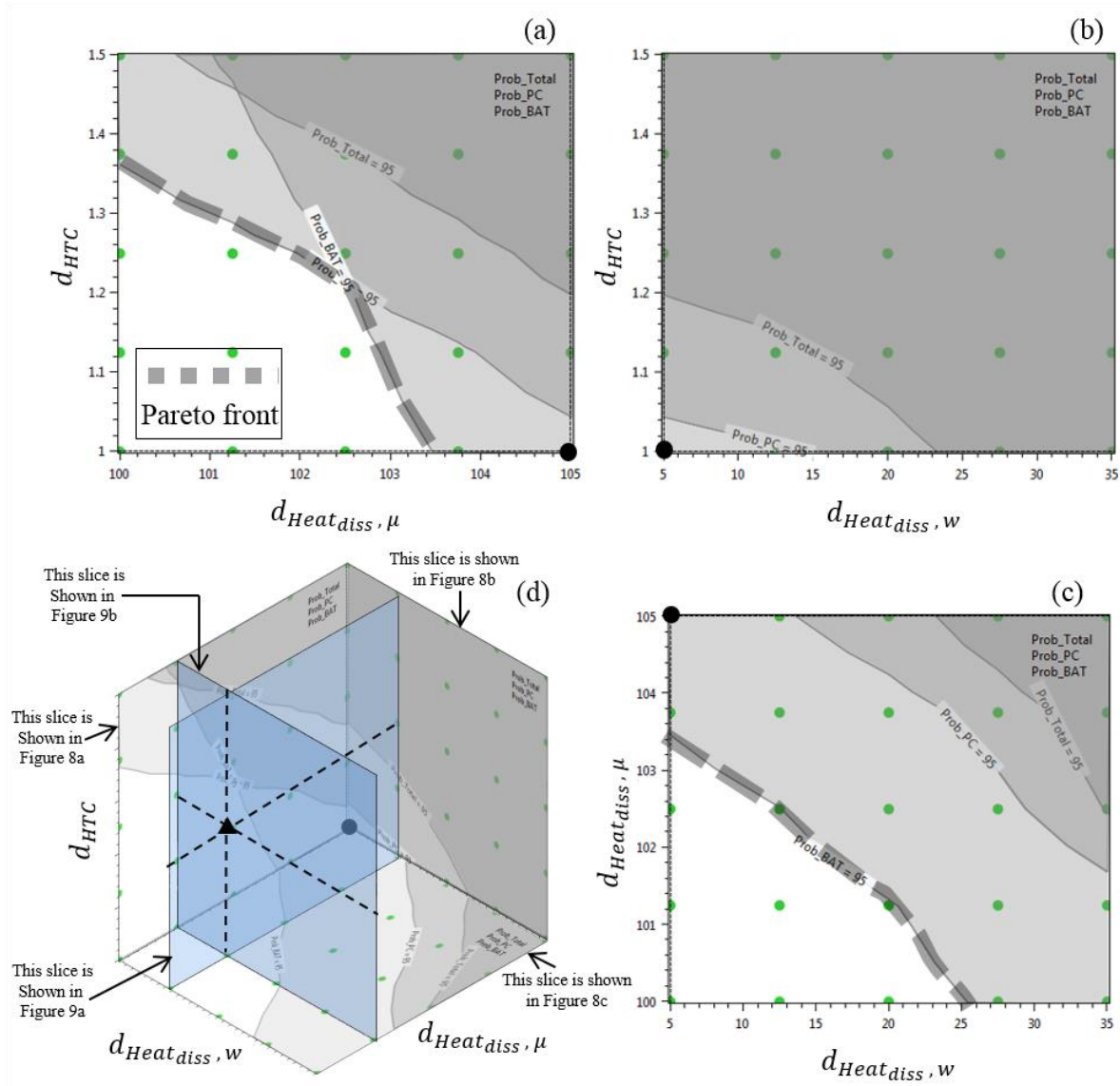


Figure 8. Slices of the trade space of the ZTM use case.

4. The design space can be explored further by visualizing different combinations of slices. These can be obtained by ‘moving’ this intersection point. The purpose of such an exploration would be to find a region of the trade space in which the Pareto front contains a combination of the parameters, \mathbf{d} , with a minimum uncertainty reduction that meets the desired probability of constraint satisfaction. A satisfactory compromise regarding the reduction of all three parameters can be seen in Figure 9, where the slices are associated with an intersection point at $\mathbf{d} = (1.25, 101.25, 12.5)$ (represented by the black triangle in Figure 8d).

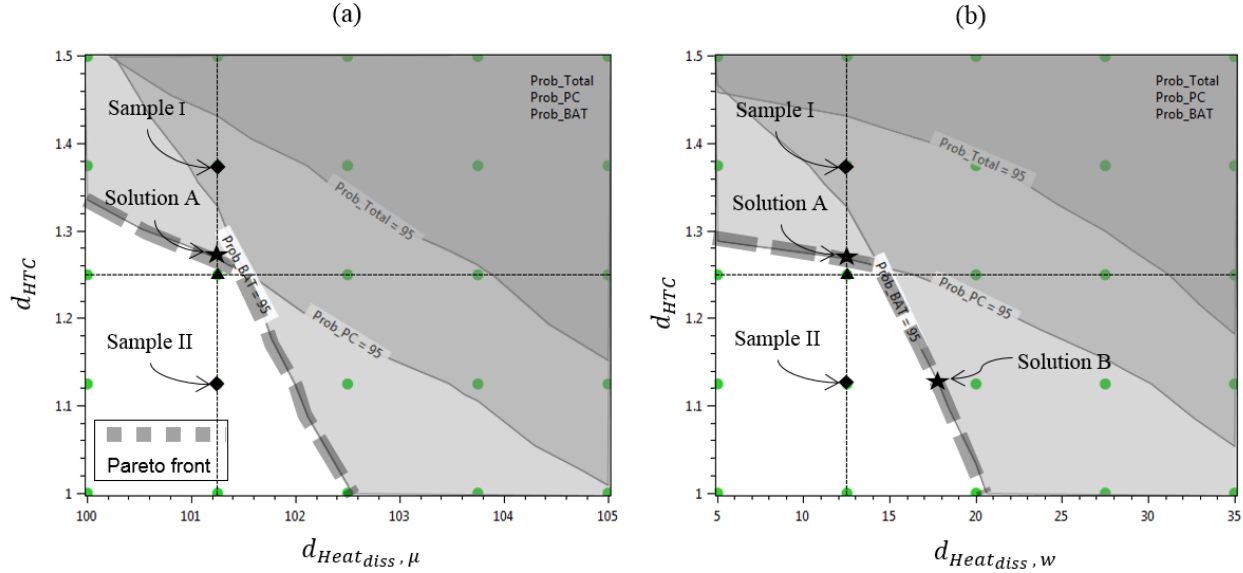


Figure 9. Tradeoff space for uncertainty allocation.

Using the new slices shown in Figure 9, the decision maker can explore possible options for allocating uncertainty to the two sources of uncertainty, by examining points from the full factorial sampling results. For example, Sample I in Figure 9 will not be chosen, since it is infeasible, i.e., only $P_{Temp_{total}}$ is satisfied, but not $P_{Temp_{PC}}$, or $P_{Temp_{BAT}}$. Sample II is a candidate, since it satisfies all constraints. However, regarding the 95% probability of constraint satisfaction, it may be reduced more than necessary. The ideal reduction will lie on the ‘Pareto front’, for example solution ‘A’ (see Figure 9a-b), or ‘B’ (see Figure 9b). Recall that a point in the trade space represents a new shape of the input PDFs. To illustrate this, the effects of selecting solution ‘A’ or ‘B’ on the shapes of the parameterized input distributions can be seen in Figure 10. As proposed in Section 3.3, such solutions can be obtained by utilizing the workflow reversal scenarios formulated at the beginning of Section 4.4.

The designer needs to decide which tradeoff strategy better suits the scenario. For this study, a tradeoff scenario was assumed where it is known that the fluctuation of the heat dissipation of the equipment will not exceed $d_{Heat_{diss}, w} = 12.5 \text{ W/m}^2$ and that the PDF could be skewed to the right with mean, $d_{Heat_{diss}, \mu} = 101.2 \text{ W/m}^2$. In such a case, it is desired to determine how much variability, d_{HTC} , is acceptable in the value of the thermal property of the materials (heat transfer coefficient) in order to guarantee a 95% probability of satisfying the thermal constraint. To answer this, the designer may choose to set up the first workflow reversal case from the two possible cases discussed at the beginning of this subsection, in order to obtain the parameters of the PDFs for allocating uncertainty. In Figure 10, the

detailed descriptions of solutions ‘A’ and ‘B’ of the Pareto front are presented. Table 5 contains a summary of the results.

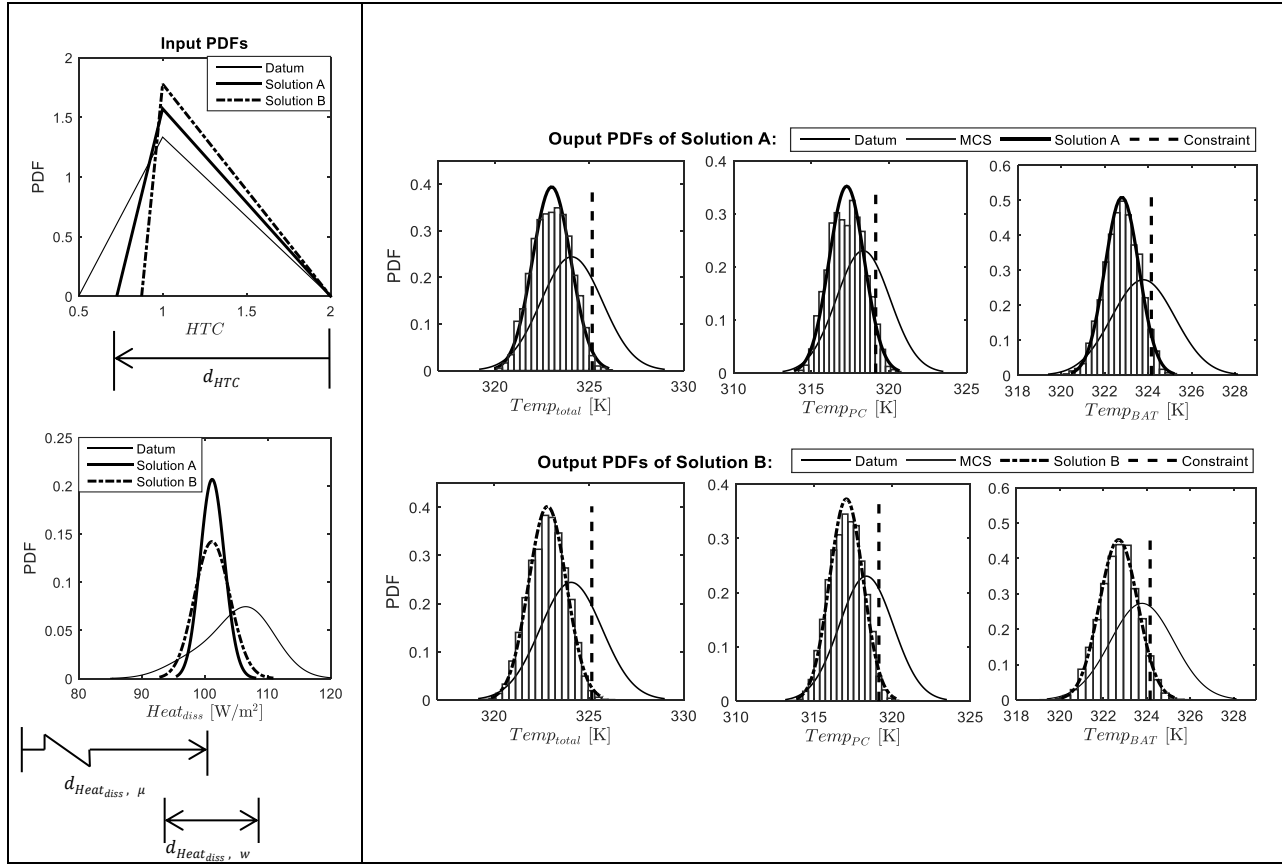


Figure 10. Results of uncertainty allocation in the ZTM use case.

Table 5. Comparison of input variability between before and after uncertainty allocation.

Allocations	Input variable HTC [$W/m^2/K$]		Input variable $Heat_{diss}$ [W/m^2]			Probability of constraint satisfaction via URQ & MCS		
	Nominal value and range of variability	d_{HTC}	Nominal value and range of variability	$d_{Heat_{diss}, w}$	$d_{Heat_{diss}, \mu}$	$P_{Temp_{total}}$	$P_{Temp_{PC}}$	$P_{Temp_{BAT}}$
Datum	1 -50% /+100%	1.5	105 [85,102]	35	105	74.78%	67.99%	60.15%
Solution A	1 -27.3% /+100%	1.27	101.25 [95.44, 107.94]	12.5	101.25	98.309%	95%*	95.77%
Solution B	1 -12.5% /+100%	1.12 5	101.25 [92.812, 110.983]	18.169	101.25	99.065%	97.412%	95%*

5 EVALUATION

Presented in this section is a comparative study of the state-of-the art “Resource Allocation Optimization” method, developed by Opgenoord and Willcox[14][20] and the proposed approach..

5.1 QUALITATIVE COMPARISON

The problem stated in Eq. (3) is recast in order to be solved by following the ‘resource allocation optimization method’. That is, an objective function is constructed that expresses designer preferences on cost, standard deviation, and risk ($100 - P_{Rng}(\mathbf{d})$). The optimization problem is stated as follows:

$$\min_{\mathbf{d} \in \mathcal{A}} \mathcal{F}(\mathbf{d}) = \alpha \frac{100 - P_{Rng}(\mathbf{d})}{P_b} + \beta \frac{\sigma_R(\mathbf{d})}{\sigma_{R,b}} + \gamma \frac{C(\mathbf{d})}{C_b}$$

$$\text{such that } \begin{cases} 100 - P_{Rng}(\text{Range}(\mathbf{d}) \geq 3000nm) \leq P_b = 15\% \\ \sigma_R \leq \sigma_{R,b} = 40lb \\ Cost \leq C_b = 40, \end{cases} \quad (15)$$

where the designer selects the weighting factors α , β , and γ to be assigned to the risk, standard deviation of the output uncertainty, and cost, respectively. As in Ref. [14], a Pareto front was generated by running the optimization for different values of weighting factors, using the Method of Moving Asymptotes [26] (implemented in the nonlinear optimization library, NLOpt [27]) and the Gauss-Legendre Quadrature method for uncertainty propagation. The selection of weighting factors that produces the Pareto front presented in Figure 11a are 30 equally-spaced values of γ between 0.4 and 0.6, with α and β constant at $\alpha = 0.5$ and $\beta = 0$. These particular values were obtained by a trial and error process, in which different combinations of weighting factors and initial conditions for the optimization setup were attempted. It was found that several combinations of the weighting factors can lead to the same value of the objective function and some of these converged to the extreme values of the Pareto front. Therefore, the Pareto front does not have a unique set of weighting factors. For the purposes of the comparison, the Pareto front solutions were projected onto the trade/decision-space, Figure 11b. It can be seen that all the Pareto front options from Figure 11a, except for one, imply reducing uncertainty on the propulsion performance, *sfc*.

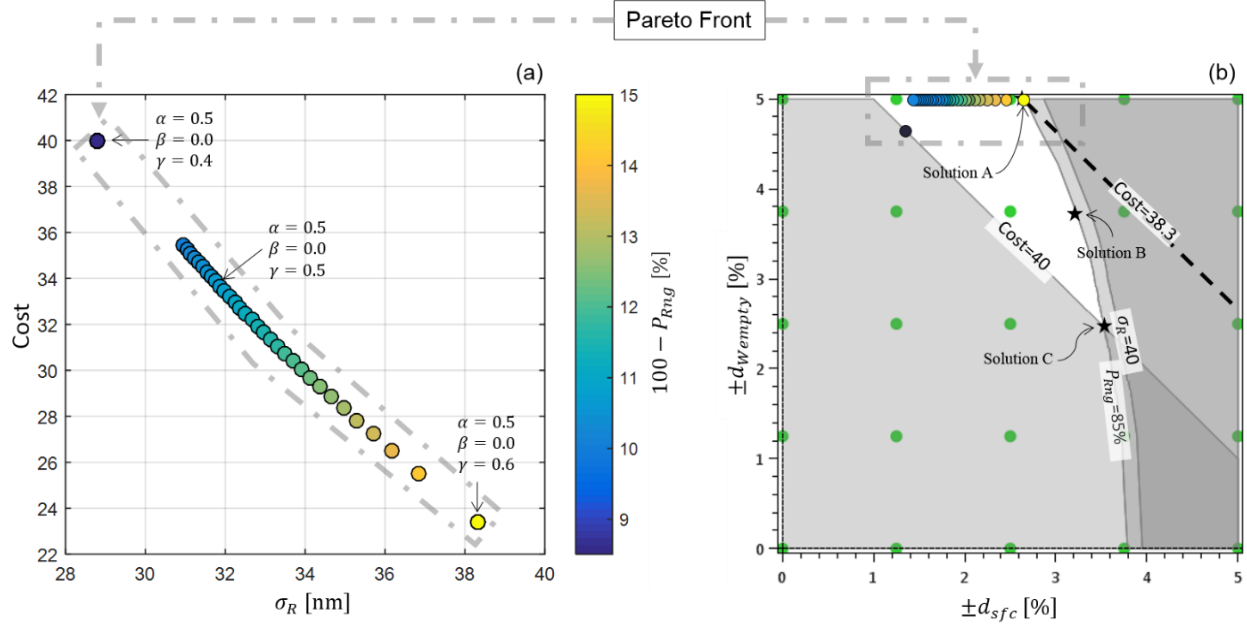


Figure 11. Pareto front projected onto a) objective space of the cost and standard deviation of range and b) design space.

A qualitative comparison of the proposed method and the ‘optimization method’ can be made by observing the results in Figure 11. With the optimization method, the Pareto front (Figure 11a) represents a set of *optimal* options for uncertainty reduction, from the perspective of a tradeoff between cost, standard deviation, and probability of constraint satisfaction. With the proposed method, the Pareto front can be identified within the feasible region. In Figure 11, the Pareto front is mapped between the objective and design spaces (highlighted by gray dash-dot rectangles). In Figure 11(b), each solution of the Pareto front can be determined by exploring the iso-contours (constraints). For example, for a given value of risk =15% ($100 - P_{Rng} = 15\%$) or $P_{Rng} = 85\%$, the minimum cost value (dotted black line) that can be achieved is located at the intersection of the cost=38.3 iso-contour and the $P_{Rng} = 85\%$ iso-contour. This intersection is at the “yellow” point at $d_{wempty} = 5\%$, $d_{sfc} = 2.66\%$, indicated as solution ‘A’. If the cost iso-contour is re-positioned, such that it intersects any other part of the iso-contour $P_{Rng} = 85\%$, the cost will always increase.

Moreover, the proposed here method provides a visualization of the entire trade space of uncertainty reduction options (as opposed to only ‘optimal’ solutions). This is significant, because in the scenario where, for example, multidisciplinary teams seek a compromise between the sources of uncertainty, the proposed method provides alternative options such as the ‘A’, ‘B’ and ‘C’ (Figure 11b). Moreover, the proposed method enables exploration of other scenarios in which the constraints can be relaxed or tightened, while guaranteeing feasible solutions, without additional computational effort.

5.2 QUANTITATIVE COMPARISON

5.2.1 Computational Efficiency with regard to the Illustrative Example (Section 2.1)

The number of simulation runs required to solve the problem stated in Eq. (3) and Eq. (15) is reported in Table 6. Since the computational time (CPU time) to solve Eq. (2) is negligible, it was not taken into account and a surrogate model is not required as proposed in Ref. [14]. As can be seen in Table 6, the proposed method performs faster than the ‘optimization method’.

Table 6. Computational cost comparison between the proposed method and the optimisation approach.

Approach	Evaluations required by the uncertainty propagation method with $n = 2$ input variables	Evaluations required by trade space visualization/ Optimization algorithms	Total number of evaluations
Proposed Uncertainty Allocation Method	URQ, $2 \cdot n + 1$, requires 5 function evaluations	DoE = $5 \cdot 5 = 25$; Gauss-Newton algorithm iterations = 3; 6 iteration in total to obtain Solution A, B and C.	$(25 + 2) \cdot 5 = 155$ model evaluations
Resource Allocation Optimization Formulation [14]	Reduced Gauss-Legendre quadratures, $\binom{n}{2} N_q^2$, with $N_q = 7$ quadrature points, requires 49 function evaluations	Number of evaluations by the optimizer algorithm to obtain the Pareto front, reported in Figure 11a, was 1577.	49 model evaluations and 1577 surrogate evaluations

5.2.2 Computational Efficiency in the Industrial Example (Section 4)

Although the ‘resource allocation optimization method’ has been demonstrated for uniform input PDFs, extension to other distribution types may be possible. To the best of our knowledge, re-casting Eq. (14) as a weighted-sum optimization problem and solved as in Ref. [14] is not possible in the case of the types of distributions listed in Table 3 (e.g., Rayleigh, non-symmetric Triangular, normal mixture). One approach maybe to formulate the optimization problem including all the statistical moments (e.g., first four moments) of other types of distributions. However, in Section 3.2, we discuss the difficulties of directly manipulating the statistical moments of the input distribution and the resulting problem of guaranteeing that the input PDFs are realizable. Shown in Table 7 is a notional comparison of the proposed uncertainty allocation method with the weighted-sum optimization problem. The computational effort to perform uncertainty propagation with the reduced Gauss-Legendre quadratures and to build the surrogate model will be 32 min. In comparison, the CPU time used to perform uncertainty propagation with the URQ method will be 44 sec, which leads to a total computational CPU time of approximately one hour and 33 minutes to solve the uncertainty allocation problem.

Table 7. Computational cost comparison between the uncertainty allocation method and the optimisation approach for the industrial example.

Approach	Uncertainty propagation method with $n = 5$ input variables — a single evaluation of the ZTM is ≈ 4 sec	Evaluations required for trade space visualization/ optimization	Estimated total number of CPU time
Proposed Uncertainty Allocation Method	URQ, $2 \cdot n + 1$, requires 11 function evaluations or 44 sec of CPU time	DoE = $5 \cdot 5 \cdot 5 = 125$; Gauss-Newton algorithm iterations = 2	$(125 + 2) \cdot 11 = 1397$, Total CPU time = 93.13 min
Resource Allocation Optimization Formulation [14]	Reduced Gauss-Legendre quadratures, $\binom{n}{2} N_q^2$, with $N_q = 7$ quadrature points, requires 490 function evaluations or 32 min of CPU time	Pareto front was not obtained	N/A

The proposed method is the most appropriate for early design stages in which models are not computationally expensive (e.g., empirical or physics-based approximations used for aircraft conceptual design [28]). If the model is expensive to evaluate (in terms of CPU time), the use of surrogate models, as proposed in Ref [14], could be used. However, the surrogate modeling process may require a large number of training points to construct an accurate surrogate [29]. Also, an important advantage of the optimization approach is that no assumptions regarding the output distributions (e.g., Gaussian) need to be made. Moreover, the proposed method will not be appropriate for problems involving distributions that require more statistical moments to describe them adequately. This is because URQ can only provide the first two moments of the output distribution.

6 SUMMARY AND CONCLUSIONS

Presented in this paper is an efficient uncertainty allocation method which utilizes (shape) parameterization of the input probability distribution functions, allowing the manipulation of several statistical moments. The method was compared with state-of-the art approaches proposed by Chen et al.[8] and Opgeenoord and Willcox[14] and was found to offer the following advantages:

- The ability to vary all the first four statistical moments of the PDF allows more freedom for exploration, and ultimately for allocating input uncertainty. Moreover, the shape parameterization enables the magnitude and spread of the uncertainty to be treated as decision variables, thereby allowing the exploration of the design space using ‘engineering’ quantities, rather than having to think in terms of statistical parameters.

- The ability to visualize the entire trade space to search for combinations of multiple input uncertainties, or PDFs, that could reduce uncertainty on multiple outputs.
- In early design stages where a surrogate model is not required, the shape parameterization, combined with efficient uncertainty propagation and inverse computation techniques, results in an efficient computational system which performs order(s) of magnitude faster, compared with an optimization technique.

When compared with the optimization approach, it was found that interactively visualizing the entire trade space not only enables several uncertainty reduction options to be explored (as opposed to only ‘Pareto optimal’ solutions), but also that other possible ‘what-if’ scenarios could be investigated. For example, multidisciplinary teams could negotiate (tradeoff) acceptable levels of uncertainty in the different sources, or could explore scenarios where the constraints can be relaxed or tightened. These can swiftly be investigated using the proposed approach.

Currently the proposed method has the following limitations:

- Although it was shown that two correlated Gaussian distributions can be transformed into an uncorrelated random space, the coordinate rotation (linear transformation) may not be generalizable with regard to other types of probability distributions. Therefore, the parameterization and the propagation methods are currently assumed to only be valid if the input probability distributions are independent.
- Although assumptions can be made regarding output distributions other than Gaussian, a study to determine appropriate approximations for other types of distributions will need to be carried out.
- With the full-factorial sampling technique, the number of samples grow exponentially with additional levels and this can impact the computational cost when visualizing the trade space.

Future work will focus on addressing the limitations listed above and also on further development of visualization and interactive techniques. Specifically, methods for dealing with correlated inputs, e.g. a transform, such as a spectral decomposition, could be used to obtain an uncorrelated set of input variables.

7 ACKNOWLEDGMENTS

The research leading to these results has received funding from the Aerospace Technology Institute in the UK, under the Advanced Product Concept Analysis Environment (APROCONe) project (Ref no. 113092). The authors gratefully thank Fabien Mangeant, Mario Cappitelli, and Michel Fouquembergh from Airbus Group Innovations for supplying the surrogate ZTM. We thank Sanjiv Sharma (Airbus-UK) for many insightful comments.

REFERENCES

- [1] De Rocquigny, E., Devictor, N., and Tarantola, S., *Uncertainty in industrial practice: a guide to quantitative uncertainty management*, John Wiley & Sons, 2008, pp 1-19. doi: 10.1002/9780470770733
- [2] Mangeant, F., "Joined initiatives around uncertainty management," *annals of telecommunications - annales des télécommunications*, vol. 66, Aug. 2011, pp. 397–407. doi: 10.1007/s12243-011-0266-7
- [3] Arbez, P., "Innovations in Aircraft Architecture Trade-off," *Seventh European Aeronautics Days*, Publications Office of the European Union, Luxemburgo, 2015, pp. 495-500.
- [4] Rouvreau, S., Mangeant, F., and Arbez, P., "TOICA Innovations in Aircraft Architecture Selection, Uncertainty Management in Collaborative Trade-offs," *6th IC-EpsMsO - 6th International Conference on Experiments/Process/System Modeling/Simulation/Optimization*, The Learning Foundation in Mechatronics (LFME), Athens, Greece: 2015.
- [5] Research Councils UK, "Advanced Product Concept Analysis Environment (APROCONe), Project Reference: 113092," *RCUK gateway* Available: <http://gtr.rcuk.ac.uk/projects?ref=113092> [retrived 8 Feb. 2018].
- [6] Oberkampf, W. L., DeLand, S. M., Rutherford, B. M., Diegert, K. V., and Alvin, K. F., "Error and uncertainty in modeling and simulation," *Reliability Engineering & System Safety*, vol. 75, Mar. 2002, pp. 333–357. doi: 10.2514/6.2001-1645
- [7] Carlsson, M., Steinkellner, S., Gavel, H., and Ölvander, J., "Utilizing Uncertainty Information in Early Model Validation," *AIAA/AAS Astrodynamics Specialist Conference , Guidance, Navigation, and Control and Co-located Conferences*, Minneapolis, Minnesota, USA: American Institute of Aeronautics and Astronautics, 2012. doi: 10.2514/6.2012-4852
- [8] Chen, X., Molina-Cristobal, A., Guenov, M. D., Datta, V. D., and Riaz, A., "A Novel Method for Inverse Uncertainty Propagation," *11th International Conference on Evolutionary and Deterministic Methods for Design, Optimization and Control with Applications to Industrial and Societal Problems, EUROGEN-2015*, Univ. of Strathclyde, Glasgow, UK: 2015, pp. 353-370.
- [9] Baumgärtel, P., Endler, G., Wahl, A. M., and Lenz, R., "Inverse uncertainty propagation for demand driven data acquisition," *Proceedings of the Winter Simulation Conference 2014*, IEEE Publ, Piscataway, NJ, 2014, pp. 710–721. doi: 10.1109/WSC.2014.7019934
- [10] Narayanan, V. A. B., and Zabaras, N., "Stochastic inverse heat conduction using a spectral approach," *International Journal for Numerical Methods in Engineering*, vol. 60, Jul. 2004, pp. 1569–1593. doi: 10.1002/nme.1015
- [11] Zabaras, N., and Ganapathysubramanian, B., "A scalable framework for the solution of stochastic inverse problems using a sparse grid collocation approach," *Journal of Computational Physics*, vol. 227, Apr. 2008, pp. 4697–4735. doi: 10.1016/J.JCP.2008.01.019
- [12] Congedo, P. M., Colonna, P., Corre, C., Witteveen, J. A. S., and Iaccarino, G., "Backward uncertainty propagation method in flow problems: Application to the prediction of rarefaction shock waves," *Computer Methods in Applied Mechanics and Engineering*, vol. 213–216, Mar. 2012, pp. 314–326. doi: 10.1016/J.JCP.2008.01.019
- [13] Fonseca, J. R., Friswell, M. I., Mottershead, J. E., and Lees, A. W., "Uncertainty identification by the maximum likelihood method," *Journal of Sound and Vibration*, vol. 288, Dec. 2005, pp. 587–599. doi: 10.1016/J.JSV.2005.07.006
- [14] Opgenoord, M. M. J., and Willcox, K. E., "Sensitivity Analysis Methods for Uncertainty Budgeting in System Design," *AIAA Journal*, vol. 54, 2016, pp. 3134–3148. doi: 10.2514/1.J054743
- [15] Padulo, M., Campobasso, M. S., and Guenov, M. D., "Novel Uncertainty Propagation Method for Robust Aerodynamic Design," *AIAA Journal*, vol. 49, 2011, pp. 530–543. <https://doi.org/10.2514/1.J050448>
- [16] Oberkampf, W., Helton, J., and Sentz, K., "Mathematical representation of uncertainty," *19th AIAA Applied Aerodynamics Conference*, 2001, p. 1645. doi: 10.2514/6.2001-1645
- [17] Helton, J. C., "Uncertainty and sensitivity analysis in the presence of stochastic and subjective uncertainty," *Journal of Statistical Computation and Simulation*, vol. 57, 1997, pp. 3–76. doi: 10.1080/00949659708811803

- [18] O'Hagan, A., and Oakley, J. E., "Probability is perfect, but we can't elicit it perfectly," *Reliability Engineering & System Safety*, vol. 85, 2004, pp. 239–248. doi: 10.1016/j.ress.2004.03.014
- [19] Padulo, M., and Guenov, M. D., "Worst-case robust design optimization under distributional assumptions," *International Journal for Numerical Methods in Engineering*, vol. 88, Nov. 2011, pp. 797–816. doi:10.2514/1.J050448
- [20] Opgenoord, M. M. J., Allaire, D. L., and Willcox, K. E., "Variance-Based Sensitivity Analysis to Support Simulation-Based Design Under Uncertainty," *Journal of Mechanical Design*, vol. 138, Sep. 2016, pp. 111410–111412. doi: 10.1115/1.4034224
- [21] Jacobs, I. M. and Wozencraft, JM., *Principles of communication engineering*, New York, Wiley, 1965. pp. 148-155
- [22] McLachlan, G., and Peel, D., *Finite mixture models*, New York, USA: John Wiley & Sons, 2004. doi: 10.1063/1.1680571
- [23] Balachandran, L. K., and Guenov, M. D., "Computational workflow management for conceptual design of complex systems," *Journal of Aircraft*, vol. 47, 2010, pp. 699–703. doi: 10.2514/1.43473
- [24] Riaz, A., "A Set-Based Approach to Passenger Aircraft Family Design," PhD Thesis, Cranfield University, 2015.
- [25] Cukier, R. I., Fortuin, C. M., Shuler, K. E., Petschek, A. G., and Schaibly, J. H., "Study of the sensitivity of coupled reaction systems to uncertainties in rate coefficients. I Theory," *The Journal of Chemical Physics*, vol. 59, 1973, pp. 3873–3878. doi: 10.1063/1.1680571
- [26] Svanberg, K., "A Class of Globally Convergent Optimization Methods Based on Conservative Convex Separable Approximations," *SIAM Journal on Optimization*, vol. 12, Jan. 2002, pp. 555–573. doi: 10.1137/S1052623499362822
- [27] Johnson, S. G., "The NLOpt Nonlinear-Optimization Package," Cambridge, MA: <http://ab-initio.mit.edu/nlop>, 2010. [retrieved 21 Nov. 2018]
- [28] Raymer, D. P., *Aircraft design: A conceptual approach*, Reston, VA: American Institute of Aeronautics and Astronautics, 2012. Chap. 3. doi: 10.2514/4.869112
- [29] Forrester, A., Sobester, A., and Keane, A., *Engineering design via surrogate modelling: a practical guide*, Chichester, West Sussex: John Wiley & Sons, 2008. Chap. 2.

2019-11-20

Interactive uncertainty allocation and tradeoff for early-stage design of complex systems

Molina-Cristobal, Arturo

AIAA

Molina-Cristobal A, Guenov M, Riaz A, van Heerden ASJ. (2020) Interactive uncertainty allocation and tradeoff for early-stage design of complex systems. AIAA Journal, Volume 58, Issue 3, March 2020, pp. 1356-1368

<https://doi.org/10.2514/1.J058442>

Downloaded from Cranfield Library Services E-Repository